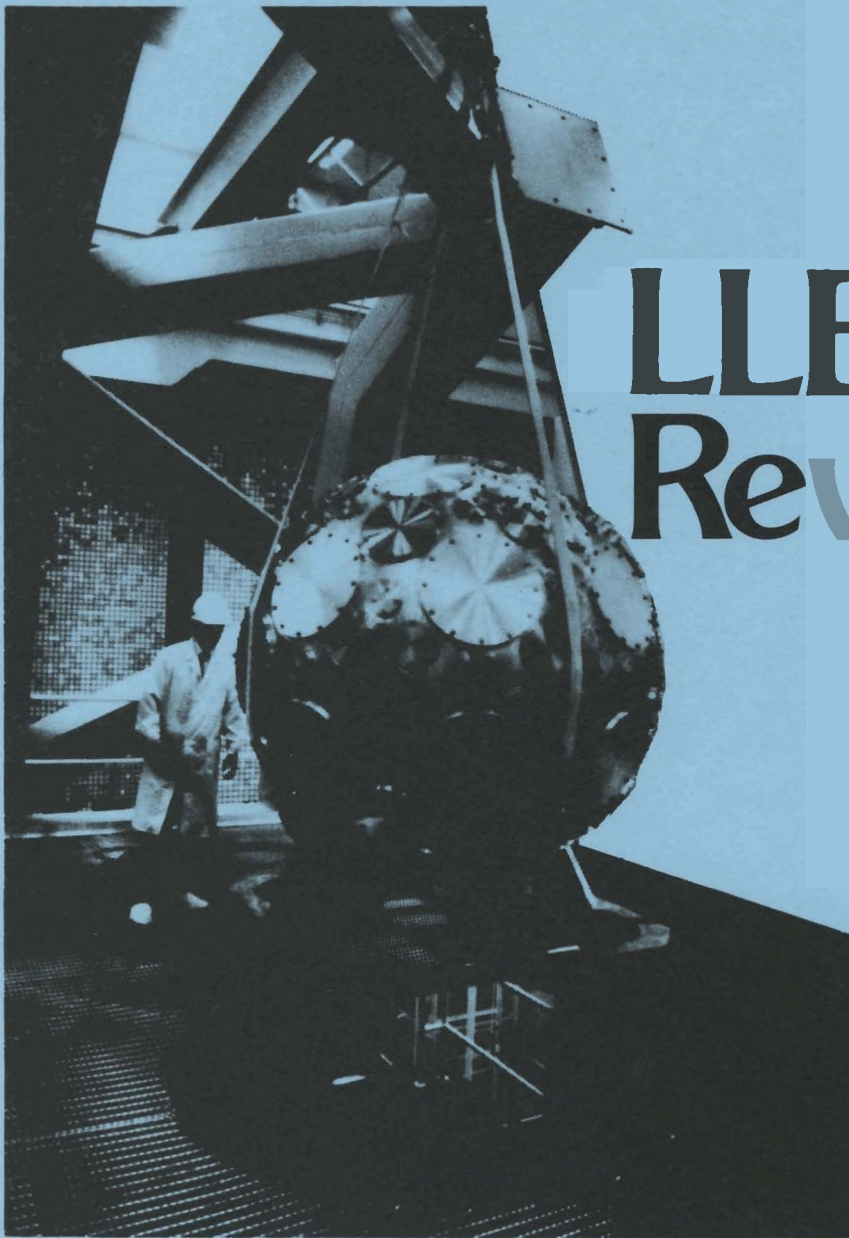


Volume II



# LLE Review

December, 1979 – February, 1980

Laboratory for Laser Energetics  
College of Engineering and Applied Science  
University of Rochester  
250 East River Road  
Rochester, New York 14623



Volume II

# LLE Review

*Editor:* **E. I. Thorsos**  
(716-275-5164)

**December, 1979 – February, 1980**

Laboratory for Laser Energetics  
College of Engineering and Applied Science  
University of Rochester  
250 East River Road  
Rochester, New York 14623





# IN BRIEF

The 24 beam OMEGA laser system has successfully completed a performance test for the Department of Energy. An output power of 12.2 TW in a short pulse and an output energy of 1.76 kJ in a long pulse have been demonstrated.

The short wavelength conversion program has made rapid progress. Nd:glass laser output ( $\lambda = 1.054 \mu\text{m}$ ) has been frequency doubled with an efficiency of over 80%.

After the period December, 1979 through February, 1980, several significant events have occurred.

- The Department of Energy has tentatively approved the OMEGA laser system performance test. Official confirmation is expected in the near future.
- The wavelength conversion program has obtained frequency tripling conversion efficiencies of over 75%.



# CONTENTS

	<i>Page</i>
IN BRIEF.....	iii
CONTENTS .....	v
Section 1. LASER SYSTEMS REPORT .....	1
1.A OMEGA Laser System .....	1
1.B OMEGA Laser System Performance Test .....	1
1.C Glass Development Laser (GDL) .....	3
Section 2. PROGRESS IN LASER FUSION .....	5
2.A Laser Wavelength Conversion Program at LLE .....	5
2.B Laser Plasma Interaction Experiments .....	6
2.C Intermediate Density Experiments on ZETA .....	8
2.D High-Density Effects on Thermonuclear Ignition for Inertially Confined Fusion.....	9
Section 3. DEVELOPMENTS IN PICOSECOND ELECTRO-OPTICS .....	12
3.A Electro-Optic Prepulse Suppression at LLE .....	12
3.B Picosecond Switching of a Multi-Kilovolt DC Bias with Laser Activated Silicon at Low Temperature .....	14
Section 4. NATIONAL LASER USERS FACILITY NEWS .....	15
PUBLICATIONS AND CONFERENCE PRESENTATIONS .....	16
REFERENCES .....	18

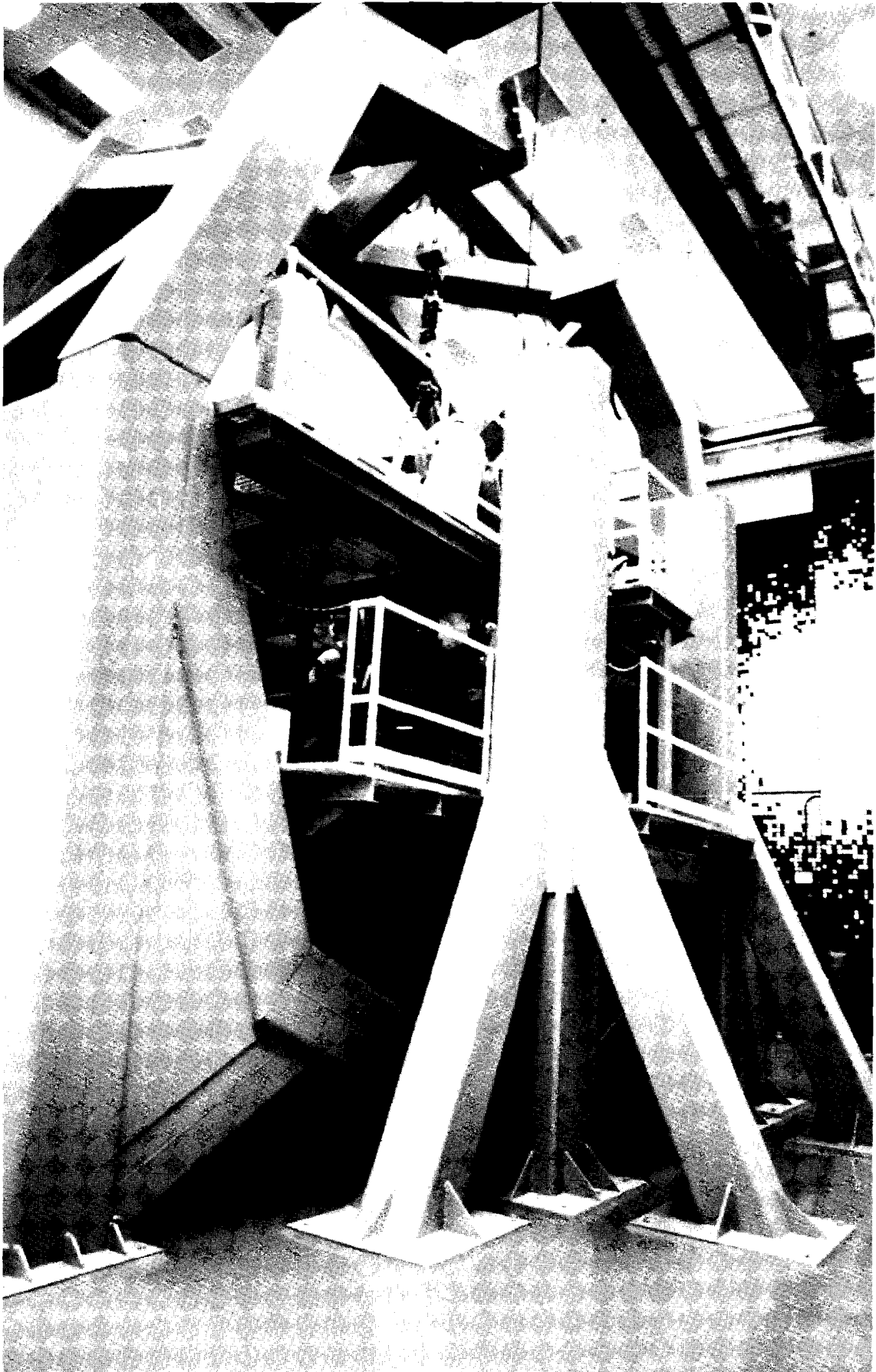


*Figure 1 OMEGA target structure, February, 1980.*

# Section 1 LASER SYSTEMS REPORT

## 1.A OMEGA Laser System

The principle activity on the OMEGA laser system during the past quarter was the 24 beam system performance test completed in January and described in a special report below. The ZETA beamlines (6 of the 24 OMEGA beamlines) were consequently not available for ZETA target experiments during this period. In February, work commenced on reactivating the ZETA system for experiments during the next quarter.

In the OMEGA target area, Figure 1, the secondary personnel platform was installed and final painting of the main structure was completed. The OMEGA target chamber, 1.6 m in diameter with 138 ports, was placed on the support structure, Figure 2, for initial testing. As a result of this testing, some additional work has been required to insure that the port axes are pointed to the chamber center to within the required tolerances.

## 1.B OMEGA Laser System Performance Test

The OMEGA 24 beam Neodymium phosphate glass laser system ( $\lambda = 1.054\mu\text{m}$ ) at LLE has been tested for overall performance, as specified by the Department of Energy contract EY-76-C-02-2812.\* The test program was successfully concluded on January 18, 1980.

The OMEGA system test was designed to insure that the system met its laser energy and power requirements while maintaining high repetition rate and adequate beam quality for target experiments. The principle objectives and results from this performance test are given in Table 1. The system minimum requirements have been

	MINIMUM DOE REQUIREMENTS	DESIGN GOAL	OMEGA OUTPUT (1/80)
Peak Power (short pulse)	7.5 TW (50 psec)	12-14 TW (50 psec)	12.2 TW (53 psec)
Energy (long pulse)	1.2 kJ (300 psec)	2.5 kJ (300 psec)	1.76 kJ (273 psec)

Table 1 The principal objectives and results from the OMEGA laser system performance test.

\*The OMEGA laser system construction began under the DOE contract EY-76-C-02-2812. On January 7, 1980 the contract number was changed to DE-AC02-76DP-40051.

exceeded by a considerable margin while maintaining a high repetition rate. Further improvements in peak power and energy are anticipated.

Before continuing with details of the DOE test series, the major characteristics of the OMEGA laser system will be reviewed. OMEGA was designed to be a high power, high energy system with an unusually high repetition rate of one shot per 30 minutes. The following features were incorporated into the system in order to reach the design goals and to hold down costs.

1. Phosphate glass rods which produce a higher specific power output than other solid state lasing materials, while maintaining rapid cool down characteristics.
2. Beam propagation with circularly polarized light to reduce the nonlinear index of refraction of the laser glass and therefore reduce high power beam breakup.



Figure 2 Placement of OMEGA target chamber on its support structure.

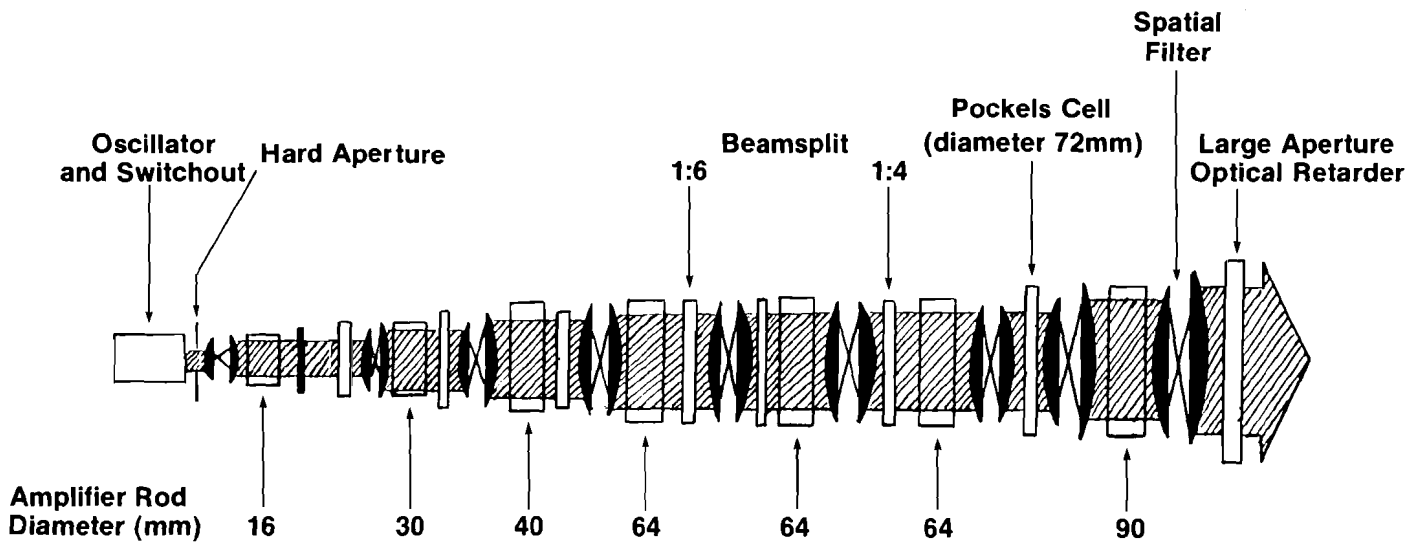


Figure 3 Staging diagram for OMEGA beamline.

3. Amplifier rods and flashlamp units of modular design which simplifies component replacement and minimizes the number of spare parts stored.
4. Full computer control of the laser charging system (power conditioning) to provide efficient operation.

A staging diagram for an OMEGA beamline is shown in Figure 3. The major elements are as follows:

1. An actively-passively mode-locked oscillator capable of producing pulse trains with a single pulse duration between 50 and 500 psec.
2. A Pockels cell switch-out system employing fast optically triggered switching (see 3.A) to select one pulse from the mode-locked train and send it into the amplifier chain. This eliminates all prepulse suppression dye cells which are commonly used in laser systems.
3. Hard aperture input to the amplifier chains, i.e., a Gaussian beam profile truncated near the 1% level. This eliminates damage sensitive soft apertures.
4. Spatial filter relaying of the image of the hard aperture throughout the laser system. This technique preserves beam quality by reducing small scale ripple growth and Fresnel ring formation.
5. Seven stages of amplification with high repetition rate rod amplifiers 16 to 90 mm in diameter with an overall gain in excess of  $3 \times 10^9$ .
6. Beam splitting 1 to 6 then 1 to 4 to reach the total of 24 beams.
7. A large aperture Pockels cell to reduce Amplified Spontaneous Emission (ASE) to a value below the design limit.
8. Large aperture optical retarder (a polarizer and wave plate) to prevent the backreflected beam from the target from re-entering the laser system. The large aperture Pockels cell acts as a back-up system for this function also.

In order to certify the OMEGA system repetition rate requirement, the performance test consisted of two shot volleys, where a volley is a series of five consecutive

shots with all 24 beams firing simultaneously and with a time interval between shots of 30 minutes or less. The first volley tested high energy output of the system with long pulses ( $264 \pm 15$  psec FWHM), while the second volley tested high power output with short pulses ( $55 \pm 5$  psec FWHM). The elapsed time between shots for these volleys is collected in Table 2, which demonstrates a repetition rate in excess of one shot per 30 minutes.

Figures 4 and 5 show, respectively, the OMEGA system energy output on the long pulse series and power output on the short pulse series. The beam balance was being adjusted during these tests. For the series of long pulses, the standard deviation of beam energies about the mean was  $\pm 18\%$ ; this was reduced to  $\pm 11\%$  for the short pulse series. Experience with the 6 beam ZETA system suggests that a beam balance of  $\pm 7\%$  (standard deviation) is a realistic expectation for OMEGA.

The temporal and spatial beam quality exceeded DOE specifications. The full angle beam divergence averaged  $153 \mu\text{rad}$  for the high energy shots and  $160 \mu\text{rad}$  for the

Table 2 OMEGA twenty-four beam performance test firing rate data.

SHOT NUMBER	ELAPSED TIME FROM PREVIOUS SHOT (MIN.)
3606	Start
3607	27
3608	28
3609	29
3610	27
3641	Start
3642	28
3643	28
3644	28
3645	27

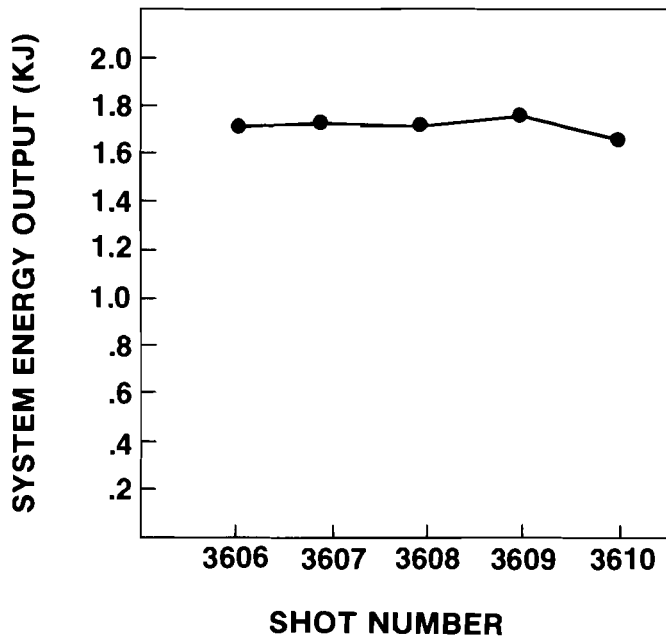


Figure 4 OMEGA energy output on long pulse series ( $264 \pm 15$  psec FWHM).

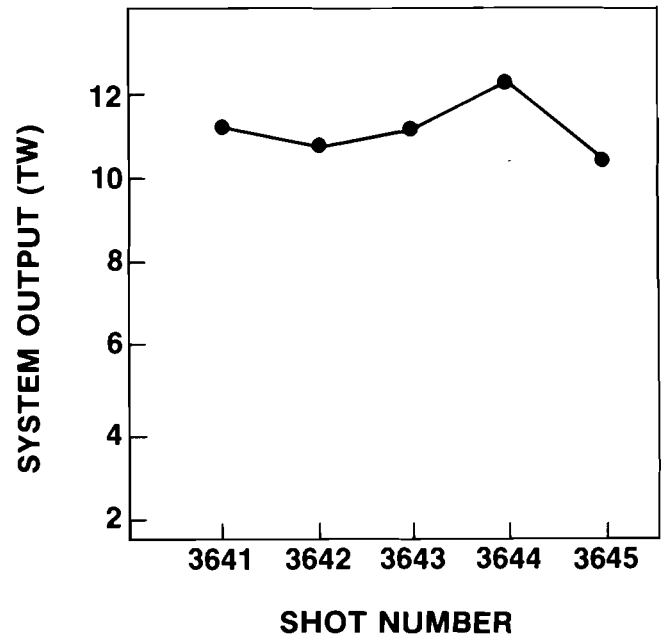


Figure 5 OMEGA power output on short pulse series ( $55 \pm 5$  psec FWHM).

high power shots. The DOE requirement was  $< 400 \mu\text{rad}$ . These results translate into equivalent focal spot diameters (90% energy diameter) for OMEGA focusing lenses (f/3) of  $92 \mu\text{m}$  for high energy shots and  $96 \mu\text{m}$  for high power shots. Therefore, the energy and power parameters measured on this test are certainly focusable onto fusion targets. The minimum target diameter presently contemplated for OMEGA is  $110 \mu\text{m}$ .

Output near field beam profiles for a representative high energy and high power shot from this test series are shown in Figures 6 and 7, respectively. The characteristic "worm" pattern of high power lasers due to small scale ripple growth is evident. The degree of ripple growth is indicated by the magnitude of the fluctuations about the radially averaged profile. The present results are considered good. The residual ring structure in the radial averaged profile is due to passage of the beam through the initial hard aperture and subsequent spatial filter pinholes, and is predicted by our Fresnel diffraction code.

The high energy, long pulse shot (Figure 6) exhibits a radially averaged profile with about a factor of three intensity variation from the center to the edge of the beam. To obtain the desired uniform radial profile, the spatial profile of the pulse entering the amplifier chain must be shaped so that when convolved with all the gain profiles of the amplifiers, the pulse emerges from the final amplifier with a uniform spatial profile. This can be quantified by the fill factor, which is a measure of the efficiency of energy extraction from the final amplifier and has a theoretical limit of 1.0. During the DOE test the fill factor was 0.60-0.65. Computer simulations indicate that a more uniform output spatial profile corresponding to a fill factor of 0.80 should be attainable on OMEGA. This would be especially important for long pulses where the energy output is limited by coating damage. Since the peak intensity must be maintained below the coating damage threshold, a more uniform radial beam profile

(higher fill factor) will permit higher energy output. Higher peak power output would also result in short pulses. Steps are presently being taken to improve the fill factor on the OMEGA beams.

Another measure of beam quality is provided by temporal characteristics of the pulse. Streak camera measurements were taken before and after the main amplification stages (in Figure 3, at the 1 to 6 beam split, and after the last spatial filter) and show smooth, near Gaussian temporal shapes exhibiting no beam breakup. For high power shots, most susceptible to beam breakup, the pulse widths agree to within 6%, an indication of good temporal beam quality.

Finally, the pulses in this test had exceedingly high contrast (main pulse energy/prepulse energy) due to the fast optically triggered switchout system. The prepulse energy per beam (excluding ASE) was less than the detection threshold of  $\sim 0.1 \mu\text{J}$ . This corresponds to a measured contrast of greater than  $7 \times 10^8$  up to 1 nsec before the pulse ( $-20 \text{ nsec} < t < -1 \text{ nsec}$ ). The contrast in the 1 nsec preceding the pulse is expected to be excellent (see 3.A). The maximum prepulse allowed by DOE specifications was  $4 \mu\text{J}$  per beam. Laser energy reaching the target at very early times ( $-100 \mu\text{sec} < t < -20 \text{ nsec}$ ) arises from Amplified Spontaneous Emission (ASE). This was measured to be  $2 \mu\text{J}/\text{beam}$ , well below expected target damage levels, even for cryogenic targets. The total pre-energy (pre-pulse plus ASE) of  $48 \mu\text{J}$  for all 24 beams was within the DOE requirements of  $< 100 \mu\text{J}$ .

### 1.C Glass Development Laser (GDL)

During the period December 1, 1979 through February 29, 1980, a total of 374 shots were taken on GDL for a variety of experiments.

**LLE REVIEW**

1. INTERACTION EXPERIMENTS: 157 shots were taken to support studies of fast ion production, suprathermal electron generation, and Brillouin backscatter and sidescatter.
2. SHORT WAVELENGTH CONVERSION PROGRAM: 137 shots were utilized in frequency doubling and tripling experiments with type II KDP crystals.
3. OMEGA BOOSTER PROGRAM: 74 shots were taken for experiments with a 17 cm diameter double pass active mirror. The beam diameter employed was 15 cm.
4. X-RAY GROUP: 6 shots were taken for crystal spectrometer diagnostic development.

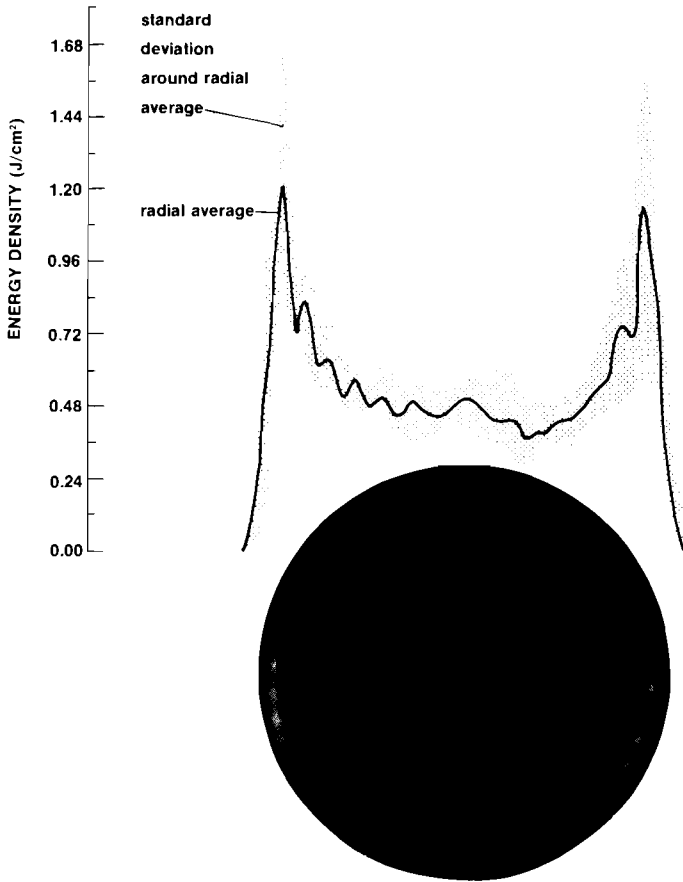


Figure 6 Near field beam profile for high energy, long pulse shot on OMEGA (shot 3606).

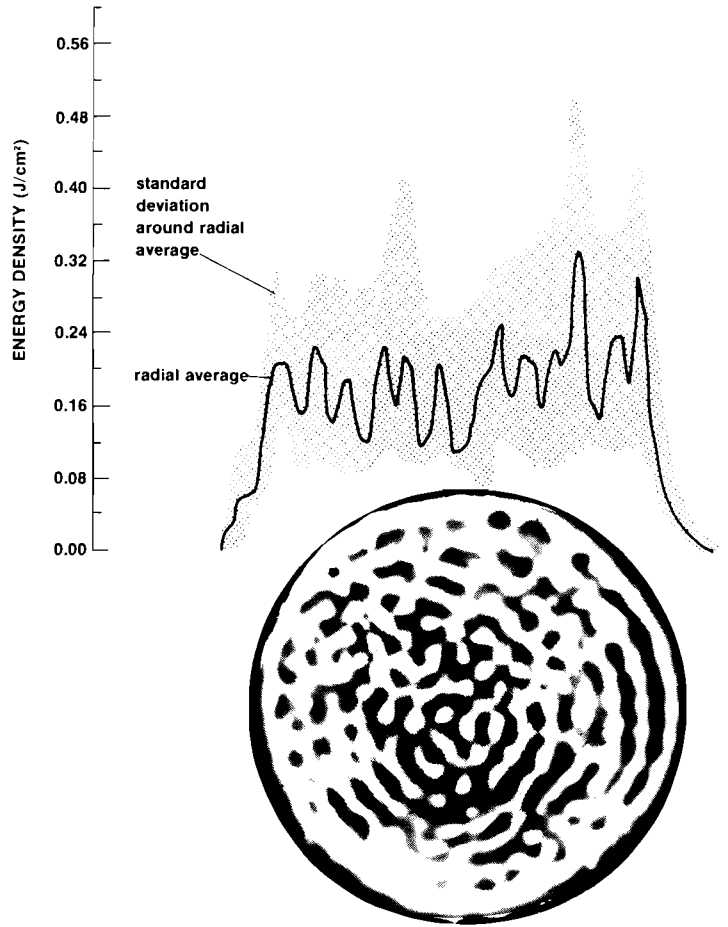


Figure 7 Near field beam profile for high power, short pulse shot on OMEGA (shot 3645).

## Section 2

# PROGRESS IN LASER FUSION

### 2.A Laser Wavelength Conversion Program at LLE

The majority of laser fusion experimentation to date has been undertaken with Nd:glass lasers ( $\lambda = 1.054 \mu\text{m}$ ) or  $\text{CO}_2$  lasers ( $\lambda = 10.6 \mu\text{m}$ ). There has been increasing interest, however, in shorter wavelength drivers, since they appear to offer significant advantages. Absorption of high intensity laser radiation is accompanied by production of energetic (suprathermal) electrons which may preheat the DT fuel. Since the preheat raises the fuel adiabat, the high fuel density necessary for ignition is more difficult to achieve. The net result is larger target and driver energy requirements for high gain targets. Considerable theoretical and experimental work has shown<sup>1</sup> that the effective suprathermal temperature,  $T_H$ , scales as  $(I \lambda^2)^n$  with  $n = 0.4 \pm 0.1$ . Since the suprathermal electron range in the target wall scales as  $T_H^{-2}$ , substantial fuel preheat reduction can be made by reducing  $\lambda$  by a factor of 2-3. The alternative of reducing the laser intensity  $I$  leads to target designs more susceptible to Rayleigh-Taylor instabilities. Reducing  $\lambda$  (or  $I$ ) will also increase the laser light absorption fraction.

Because of the considerable potential of shorter wavelength drivers, a wavelength conversion program has been initiated at LLE to study the feasibility of converting the Nd:glass laser output ( $\lambda = 1.054 \mu\text{m}$ ) by frequency doubling and tripling ( $\lambda = 0.53 \mu\text{m}$ ,  $0.35 \mu\text{m}$ ) with KDP (potassium diphosphate) crystals<sup>2</sup>. Conversion to even shorter wavelengths would lead to problems with absorption in the focusing elements (for target irradiation) and has not been pursued. At the present time, conversion from  $\lambda = 1.054 \mu\text{m}$  is far more practical than direct use of shorter wavelength lasers. The program to date has involved experimental conversion studies on the GDL laser system with laser intensities appropriate for high power target irradiation. Accompanying this, a substantial theoretical effort has yielded a computer code (MIXER) with the capability of making detailed simulations of the wavelength conversion process. The progress to date has been very encouraging: doubling efficiencies greater than 80% and preliminary high tripling efficiencies have been obtained in remarkable agreement with MIXER simulations. At LLE the most likely application to future laser fusion studies will be with frequency tripled light ( $\lambda = 0.35 \mu\text{m}$ ). Compared to experiments with unconverted light, the loss of laser energy in conversion is expected to be far more than compensated by improved absorption and target performance with the shorter wavelength light.

Frequency tripling is carried out as a two step process with KDP crystals. First, part of the initial beam at frequency  $\omega$  is doubled to  $2\omega$ . The remaining amount at  $\omega$  is mixed with the  $2\omega$  component to yield  $3\omega$  in the second

step. The initial LLE conversion experiments were frequency doubling experiments with the goal of optimizing the output for the tripling step to follow. The doubling results will be discussed here, while the tripling work (still underway at the end of this quarter) will be described in more detail at a later date. A particularly important fact for the frequency doubling strategy is that the optimum intensity ratio of  $2\omega$  to  $\omega$  for input to tripling is 2 to 1; that is, equal photon numbers of  $\omega$  and  $2\omega$  light. Therefore, the desired conversion efficiency from  $\omega$  to  $2\omega$  is 67% if a tripling step is to follow.

There are a number of factors which contribute to the conversion efficiency of a crystal:

- Crystal cut
- Crystal length and area
- Crystal alignment (tilt angle)
- Beam spatial and temporal profile
- Crystal temperature
- Coating and materials damage limitations

Factors a-e have been studied with the aid of the computer code MIXER as a very important guide for these experiments. This has made possible a rapid optimization of these factors.

The choice of crystal cut is very important. There are two options here, referred to as type I and type II conversion. See Figure 8. (In type I doubling, the components of the incident E vector are both along the ordinary axes of the crystal, and maintain their relative phase while propagating through the crystal. In type II doubling, a component of the incident E vector lies along the extraordinary axis of the crystal; the components therefore do not stay in phase while propagating through the crystal.) We have concentrated on type II doubling for several reasons. The alignment and pointing requirements for a type I doubling crystal are a factor of two more stringent than for a type II crystal of the same dimensions. Additionally, a type I crystal must be a factor of 1.35 thicker than a type II crystal to yield the same conversion efficiency at the same intensity. The type I crystal is therefore a factor of 2.7 more sensitive to pointing error or beam divergence. Also, it is possible to cut a larger diameter type II than type I crystal from the same raw crystal. This would become especially significant for multi-beam fusion applications of frequency conversion.

The initial frequency conversion experiments with the GDL laser system have been limited to a 60 mm diameter beam, since the KDP crystals on hand had a 64 mm aperture. The tests were carried out at the output of the last 64 mm rod amplifier of GDL. The energy available at this point in the system was 22J in 140 psec (FWHM).

Figure 9 gives measured energy conversion efficiencies to the second harmonic ( $2\omega$ ) as a function of incident

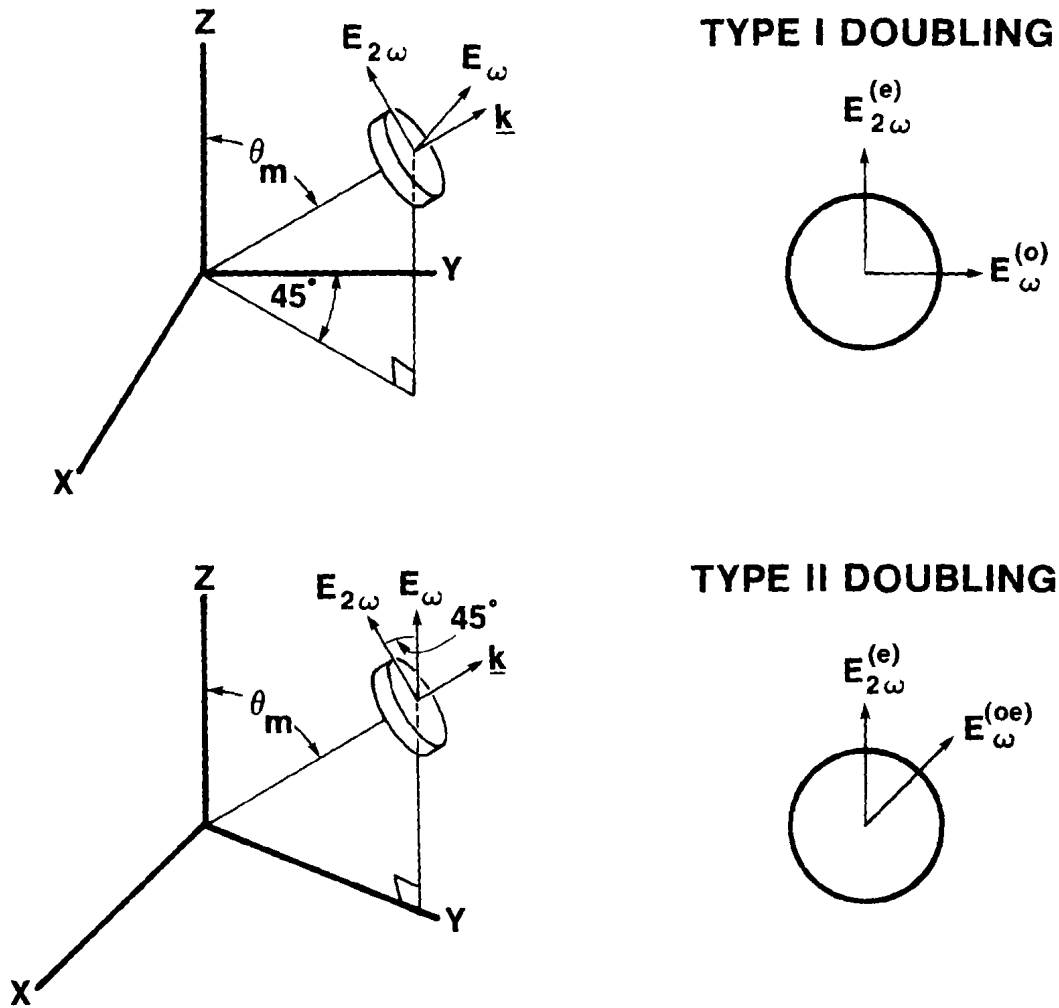


Figure 8 Type I and type II doubling with KDP crystals. In both cases, the Z axis is the extraordinary (optic) axis of the crystal while the X and Y axes are the ordinary axes of the crystal. The propagation direction of all waves is given by the vector  $\mathbf{k}$ . In type I doubling, the incident E vector of frequency  $\omega$  has only ordinary components. In type II doubling, the incident E vector has a component along the extraordinary direction.

intensity for several tilt angles  $\Delta\theta$  of the crystal. It can be seen that for  $\Delta\theta=0$ , conversion efficiencies to  $2\omega$  of over 80% are obtained. These results are in excellent agreement with predictions of the code MIXER. Beam spatial and temporal profiles are incorporated into these simulations. When the crystal is tilted slightly, the conversion efficiency drops, again in very good agreement with MIXER. One way of obtaining the optimum 67% conversion efficiency to  $2\omega$  (for later conversion to  $3\omega$ ) is to tilt the crystal about 0.6 mrad as indicated in Figure 9. By doing this, the correct conversion efficiency is obtained, and the response is relatively insensitive to intensity which is advantageous if there are spatial variations in the beam profile. The results obtained to date ( $> 80\%$  conversion to  $2\omega$ ) coupled with the superb agreement between simulation and experiment are very encouraging. Preliminary results for  $3\omega$  conversion appear equally promising. The prospects for short wavelength laser fusion experiments are good.

## 2.B Laser Plasma Interaction Experiments

Basic studies of the laser plasma interaction are continuing on the GDL laser system at LLE. During this quarter, two consequences of energetic (suprathermal) electron production during high intensity laser light absorption have been studied: hard x-rays and fast ions. By measuring these signatures of suprathermal electrons, properties of the suprathermal distribution can be inferred, such as the effective suprathermal temperature,  $T_H$ . These experiments examined the effect on  $T_H$  of a carefully controlled prepulse of variable energy preceding the main 50 psec pulse. The properties of the suprathermal distribution are of considerable importance to laser driven implosions. If an excessive amount of the absorbed energy appears in very energetic electrons, detrimental preheat of the DT fuel can occur. Energetic electrons also

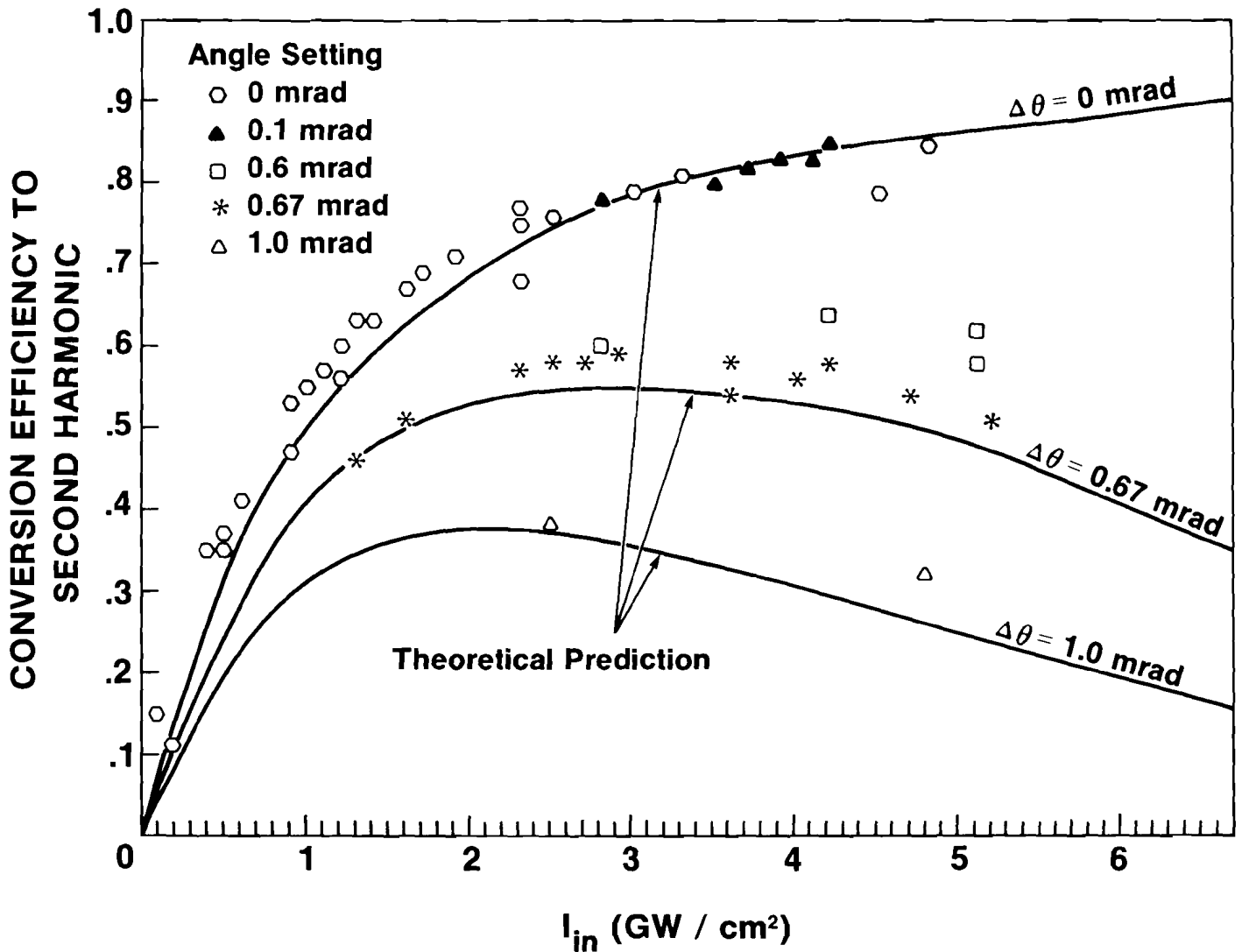


Figure 9 Frequency doubling energy conversion efficiencies obtained with a 12mm thick type II KDP crystal on GDL for various tilt angles of the crystal. The theoretical predictions were made with the computer code MIXER.

can be efficient at accelerating fast ions outward from the target, an inefficient use of energy for driving implosions. It is therefore of some interest that in these experiments prepulses have the effect of reducing  $T_H$  and of decreasing the amount of energy in fast ions. Similar effects have been indicated by experiments elsewhere<sup>3,\*</sup>.

The GDL beam was configured for two beam irradiation and surface focused onto 80 $\mu$ m diameter (0.8 $\mu$ m wall) empty glass microballoon targets. In one set of experiments, prepulses of variable energy were introduced at either 300 or 1100 psec before the main pulse; both pulses were nominally 50 psec (FWHM). The prepulse produces a low density plasma around the target, and the prepulse/main pulse combination simulates some properties of longer pulses, e.g., longer density scale lengths. Hard x-rays were detected by a K-edge filtered spectro-

meter<sup>†</sup>. The x-ray data obtained is consistent with an energetic electron distribution, in the energy range of 10-50 keV<sup>†</sup>, which can be characterized by a single suprathermal temperature  $T_H$ . In Figure 10,  $T_H$  is given as a function of the energy ratio of the prepulse to the main pulse, where the main pulse intensity was  $\sim 5 \times 10^{15}$  W/cm<sup>2</sup>. We observe a steady drop in  $T_H$  as the prepulse energy is increased. No significant differences were noted in  $T_H$  for the two prepulse to main pulse separations.

Values for  $T_H$  were also obtained from the fast ion ( $v > 10^8$  cm/sec) spectrum obtained with a Thomson parabola.

<sup>†</sup>The spectrometer was equipped with three K edge filter channels and three lead absorber ratio channels. The latter provided information on the very energetic tail of the electron distribution (energies from 50 keV to several hundred keV), where the electron distribution has a higher population than given by an extrapolation from lower energies of a single suprathermal temperature model. Effects on the x-ray spectrum from this part of the electron distribution could then be eliminated in the determination of  $T_H$ .

\* It has been a common observation at many laboratories that unintentional prepulses on target implosions reduce the energy in fast ions and the neutron yield.

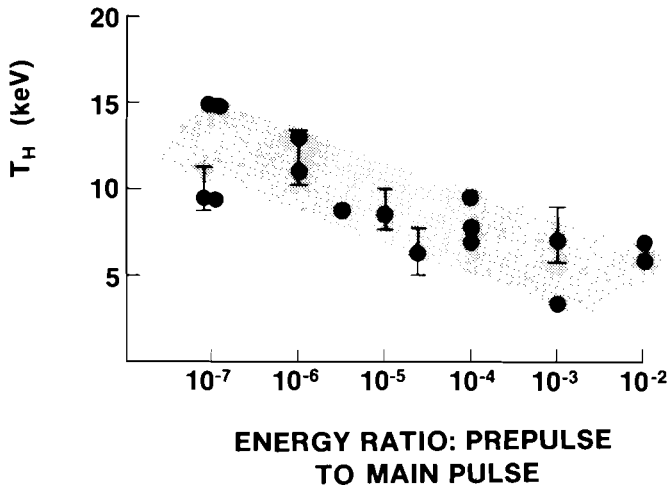


Figure 10  $T_H$  versus the energy ratio of prepulse to main pulse obtained from hard x-ray spectra. The main pulse peak intensity was  $5 \times 10^{15}$  W/cm<sup>2</sup>. Typical error bars are shown.

The ion data is consistent with an isothermal expansion model, which then yields a value for  $T_H$ . Values for  $T_H$  from fast ion spectra are typically 1.0-1.5 times the  $T_H$  obtained from hard x-ray data. Suprathermal temperatures from fast ion spectra also decline as the prepulse energy is increased; in addition, the total energy in fast ions decreases.

These results for the  $T_H$  dependence on prepulse energy conflict with crude estimates for the dependence. In previous experiments at LLE, the density profile from  $0.1 \times n_c$  to  $n_c$  (critical density) has been measured by double pulse holographic interferometry using a fourth harmonic probe pulse<sup>4</sup>. The density scale length in this region below  $n_c$  is found to increase with prepulse energy. The scale length  $L$  at  $n_c$  may also increase and certainly would not be expected to decrease with prepulse energy. Combining this observation with the scaling  $T_H \sim \sqrt{L}$  for resonance absorption<sup>5</sup> would suggest that  $T_H$  should not decrease with increasing prepulse energy. Since  $T_H$  did decrease, the processes in the corona determining  $T_H$  are clearly more complex than assumed above. A number of effects related to the transport of suprathermal electrons in the low density prepulse plasma may be important here. It is also possible that the incident intensity reaching critical density is reduced by stimulated scattering on the longer density scale lengths produced by the prepulse. This area of the laser plasma interaction certainly requires more investigation.

## 2.C Intermediate Density Experiments on ZETA

Analysis of previous implosion experiments with plastic coated targets has shown an increase in yield with wall

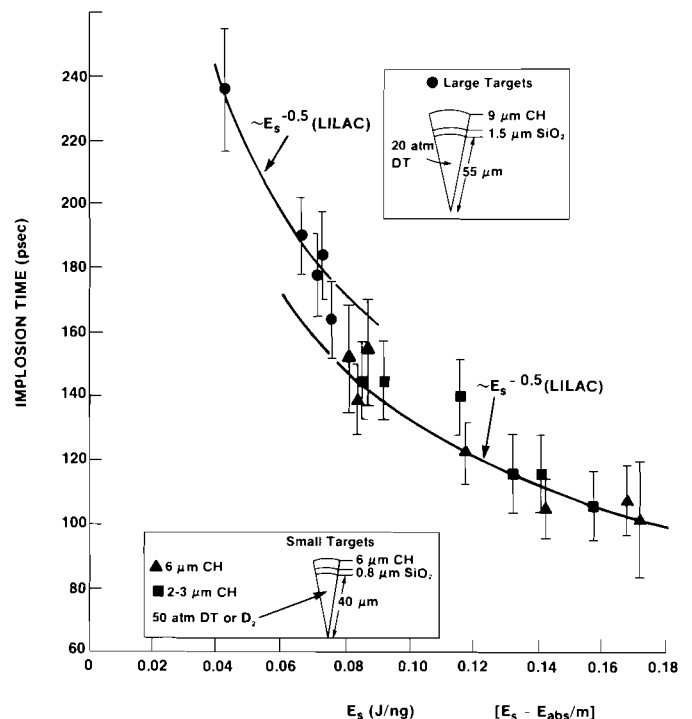
thickness for constant implosion velocity. We therefore have indication of improved yield due to higher compression, an expected consequence of symmetric implosions with thicker wall targets. These results are also reproduced by LILAC simulations.

The experiments were carried out on the ZETA six beam laser with 100-150 J of energy in 50-80 psec pulses. The implosion times were measured with an x-ray streak camera equipped with a sequence of timing fiducials, which were at a known temporal relation to the laser pulse. Measurements were then made of the time from the peak of the laser pulse to the peak of the x-ray pulse produced at stagnation of the implosion, this time being defined as the implosion time. Figure 11 shows implosion times versus specific absorbed energy,  $E_s = E_{abs}/m$ , for a number of experiments on two sizes of plastic coated targets.

A crude estimate for the expected implosion time scaling with  $E_s$  can be made by taking the kinetic energy of the imploding shell to be proportional to  $E_s$ . Then the implosion time  $\tau \sim v^{-1} \sim E_s^{-0.5}$ . LILAC simulations give the same scaling result. The data in Figure 11 fall along such scaling curves quite well. The larger targets lie on a separate curve because of the longer implosion distance\*. For the smaller 85-90  $\mu\text{m}$  diameter targets the plastic coating thickness was either 2-3  $\mu\text{m}$  or 6  $\mu\text{m}$ . We observe that for these targets the implosion time is independent of coating thickness for a particular  $E_s$ .

\*The difference in implosion times is also related to the fill pressure difference.

Figure 11 Implosion time versus specified absorbed energy obtained on ZETA for two sizes of targets. The curves show LILAC scalings.



the yield directly ( $Y \sim \rho_{DT}$ ) and indirectly by the increase in  $T_i$  through the extra compressional heating<sup>6</sup>. LILAC simulations also give a factor of 3 increase in yield for this wall thickness difference in very good agreement with experiment. It is very encouraging that our implosion symmetry on ZETA is sufficient to demonstrate the increase in yield with wall thickness (at constant  $E_s$ ) expected theoretically.

## 2.D High-Density Effects on Thermonuclear Ignition for Inertially Confined Fusion

To obtain net energy production with inertially confined fusion, the DT fuel must undergo thermonuclear ignition. With a sufficiently high fuel  $\rho R$  (density-radius product), the 3.5 MeV alpha particles produced in the DT reaction deposit their energy within the fuel leading to rapid self-heating (ignition). Values of fuel  $\rho R$  larger than 0.3 g/cm<sup>2</sup> and fuel plus tamper  $\rho R$  larger than 1 g/cm<sup>2</sup> have been considered to be required for a thermonuclear burn sufficient for net energy production<sup>8</sup>. The tamper is composed of relatively cold material surrounding the DT fuel and contributes to the yield by prolonging the burn time.

We have found that under some conditions, the minimum required fuel  $\rho R$  may be reduced. Alpha particles from the DT reaction have been calculated to reflect from a high-Z, Fermi-degenerate shell surrounding the fuel of inertial fusion targets. This leads to a reduction in the minimum fuel  $\rho R$  needed to sustain a thermonuclear burn, and possibly to a reduction of the minimum input energy required to achieve thermonuclear ignition<sup>9</sup>.

The amount of alpha particle reflection from the tamper is determined by competition between energy loss to electrons and Coulomb scattering by ions in the tamper. At the onset of thermonuclear burn, the tamper should ideally be Fermi degenerate for minimum ignition requirements. Since only electrons near the Fermi surface would then contribute to particle slowing down, the energy loss would be less than expected classically, and the relative amount of scattering would be enhanced, increasing the energy deposition in the fuel. This in turn results in a reduction in the minimum fuel  $\rho R$  needed to sustain a thermonuclear burn.

To find the density needed for reflection, the following test problem was solved. A DT sphere was set at  $T = 10$  keV,  $n_e = 5 \times 10^{26}$  cm<sup>-3</sup> ( $10^4 \times$  liquid density) and  $\rho R = 0.3$  g/cm<sup>2</sup>. This was surrounded by a gold shell ( $Z = 79$ ) at 1 keV whose density was varied. To determine how the energy reflection depends on tamper density, the Fokker-Planck equation was solved for the alpha-particle transport.

\*A thicker wall target also implies a thicker tamper, which leads to a longer disassembly time and therefore a longer burn time further improving the yield.

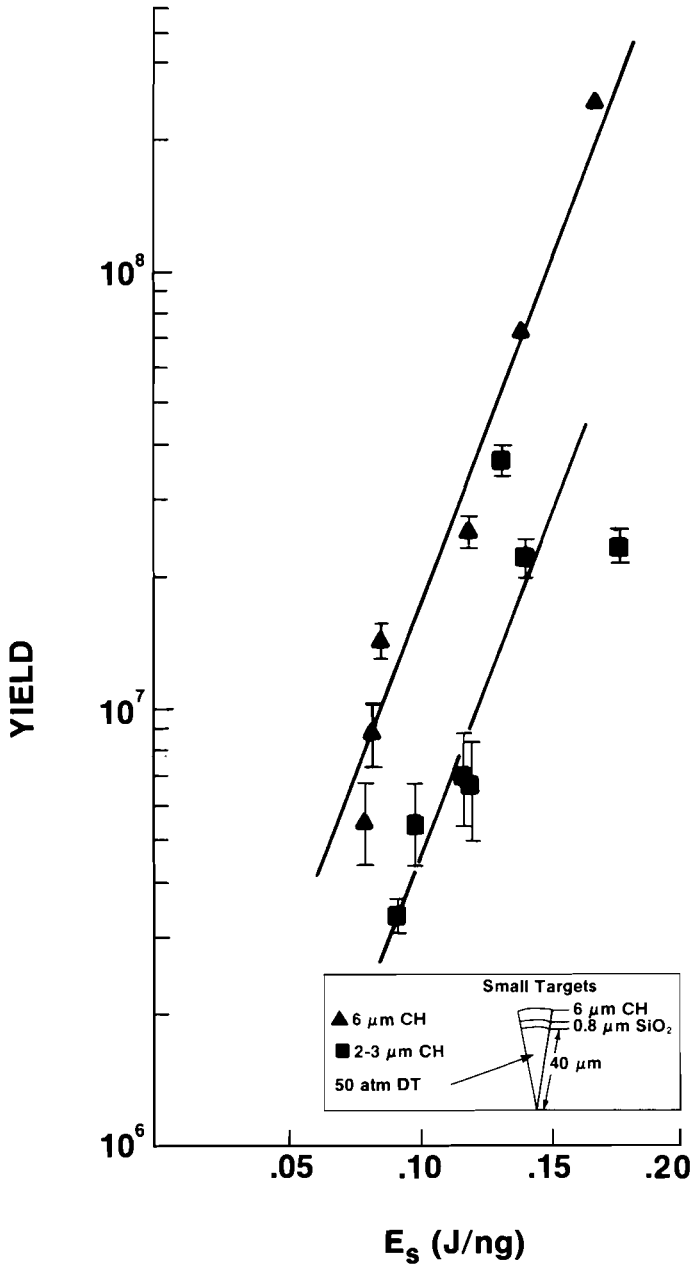


Figure 12 Neutron yield versus specific absorbed energy for the smaller diameter targets of Figure 11. The lines summarize the results for the two coating thicknesses: 6  $\mu\text{m}$  CH coatings lead to yields 3-4 times that obtained for 2-3  $\mu\text{m}$  CH coatings for the same  $E_s$ .

Figure 12 shows the yield versus  $E_s$  for the small targets only. For identical  $E_s$ , the targets with the thicker 6  $\mu\text{m}$  CH coatings have, on the average, 3-4 times the yield of the 2-3  $\mu\text{m}$  CH coated targets. The most important parameter determining the yield is the DT ion temperature  $T_i$ . Targets imploded with equal average implosion velocities to the same compression would be expected<sup>6</sup> to reach the same  $T_i$ . The yield results alone, then, suggest that these thicker wall targets reach higher compressed DT densities. The x-ray imaging results discussed previously<sup>7</sup> also support an increase in compressed DT density with increasing wall thickness. The higher density increases

## LLE REVIEW

The alpha particle scattering from the high Z ions was calculated with standard methods. For energy loss, the electrons, both bound and free, were taken as a semi-degenerate electron gas.

Results of this calculation are shown in Figure 13. Plotted is the fraction of all the alpha-particle energy (produced throughout the fuel) which is deposited back into the fuel. The effect of reflection becomes apparent as the electron density in the gold shell exceeds  $10^{27}$   $\text{cm}^{-3}$ . At  $5 \times 10^{27}$  electrons/ $\text{cm}^3$ , energy deposition in the fuel has increased by 25%. The maximum electron density in gold permitted by pressure equilibration with the fuel in this example is about  $5 \times 10^{27}$   $\text{cm}^{-3}$  from the Thomas-Fermi equation of state.

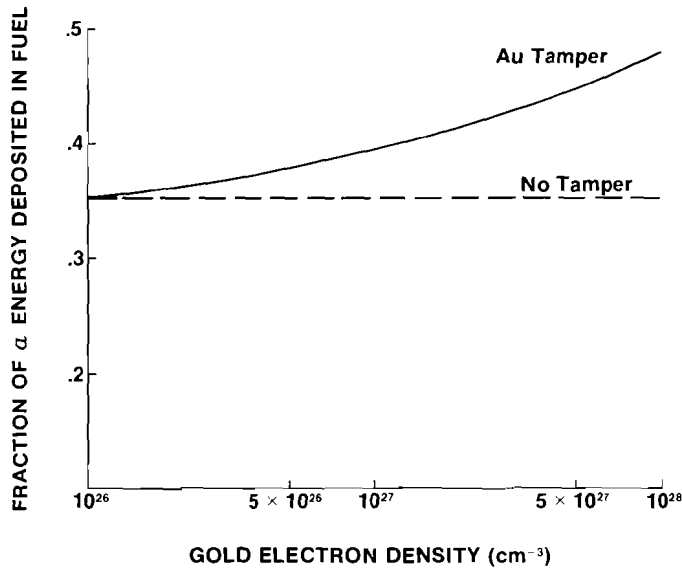


Figure 13 Fraction of alpha-particle energy deposited in the fuel as a function of density in the gold tamper. (Fuel:  $T = 10$  keV,  $n_e = 5 \times 10^{26}$   $\text{cm}^{-3}$ ,  $\rho R = 0.3$   $\text{g/cm}^2$ . Tamper:  $T = 1$  keV.)

We may note that the densities required for significant alpha particle reflection are consistent with those originally suggested<sup>10</sup> as optimum for inertial confinement fusion, but higher than more recent estimates of compressed densities for high gain targets<sup>11</sup>. When the compressed density is reduced, the size of the compressed region must increase to maintain the  $\rho R$  condition, which in turn implies larger targets and more laser energy. Therefore, driver energy requirements would be minimized if the high densities considered here are ultimately obtained.

The size of the gold tamper needed for reflection is shown in Figure 14. For these results, the tamper electron density was set at  $5 \times 10^{27}$   $\text{cm}^{-3}$ , and its  $\rho R$  was varied. (Fuel conditions remained the same as in Figure 13.) As can be seen, almost all the reflection occurs with a tamper  $\rho R$  of 0.1  $\text{g/cm}^2$ . This is much smaller than the values of  $\rho R$  ( $\sim 1$   $\text{g/cm}^2$ ) needed for energy breakeven<sup>9</sup>. The fraction of alpha-particle energy transmitted through the tamper is also shown in Figure 14. Such transmission

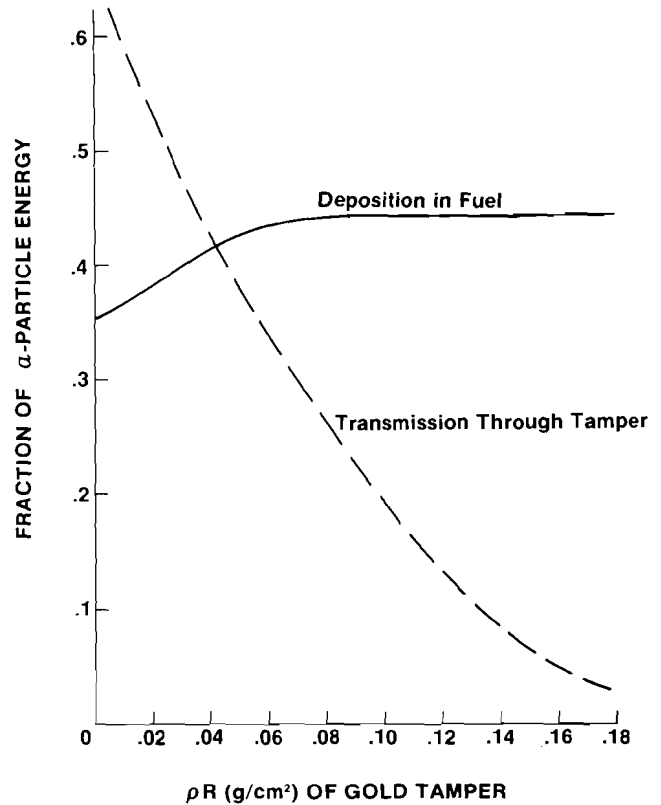


Figure 14 Fraction of alpha-particle energy deposited in the fuel and transmitted through the tamper as a function of  $\rho R$  in the tamper. ( $T = 1$  keV,  $n_e = 5 \times 10^{27}$   $\text{cm}^{-3}$ .)

could be important for double-shell target designs which require the thermonuclear burn to propagate from one DT fuel region to another, across a high-Z shell. (The fraction of energy in Figure 14 which was not deposited or transmitted was absorbed by the tamper.) If electron degeneracy had not been considered there would have been essentially no reflection and no transmission; all alpha particles escaping the fuel would have deposited their energy in the tamper.

As a final point, the reduction in  $\rho R$  needed for thermonuclear ignition is shown in Figure 15. Again, the gold tamper was set with  $n_e = 5 \times 10^{27}$   $\text{cm}^{-3}$ , but now the  $\rho R$  of the fuel was changed. The results show that if the bare fuel ignites at  $\rho R = 0.3$   $\text{g/cm}^2$ , then, for the same fractional energy deposition, it should ignite at  $\rho R = 0.22$   $\text{g/cm}^2$  with the gold tamper - a reduction of 25% in  $\rho R$ . The significance of the 25% reduction obtained for fuel  $\rho R$  is that it corresponds to almost a 50% reduction in mass of the compressed target. [The mass will vary as  $(\rho R)^2$  for fixed  $\rho$  since typically most of the mass  $M$  is concentrated in the tamper, i.e.,  $M \sim (\rho R)^2 (\rho_T \Delta R) / \rho^2$  where  $\rho_T$  and  $\Delta R$  are the density and thickness of the tamper.] However, to achieve this reduction, electron densities must reach  $\sim 5 \times 10^{27}$   $\text{cm}^{-3}$  in the tamper. Since in many target designs, the input energy varies as the compressed mass, alpha-particle reflection could lead to a substantial reduction in the driver energy needed to achieve thermonuclear ignition.

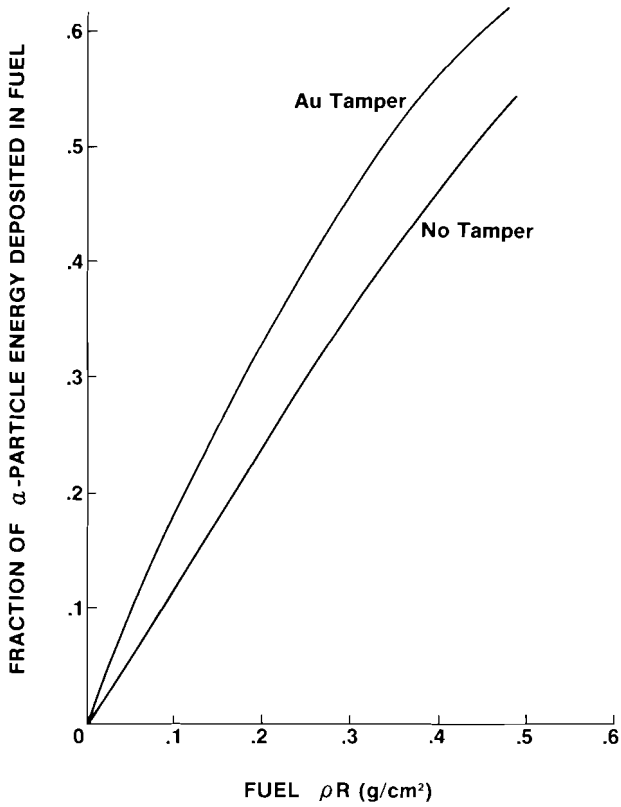


Figure 15 Fraction of alpha-particle energy deposited in the fuel for tamped and untamped pellets. (Tamper conditions  $T = 1 \text{ keV}$ ,  $n_e = 10^{27} \text{ cm}^{-3}$ .)

The results here were obtained for an idealized situation to demonstrate the possibility of alpha-particle reflection. The exact magnitude of the effect will depend on the particular target design under study.

## Section 3 DEVELOPMENTS IN PICOSECOND ELECTRO-OPTICS

### 3.A Electro-Optic Prepulse Suppression at LLE

In laser fusion experiments prepulse suppression is of pre-eminent importance, i.e., the main laser pulse must not be preceded by unprogrammed low intensity pulses. Typically, prepulse requirements are less than a few  $\mu\text{J}$  of accumulated prepulse energy over the last  $\sim 20$  nsec and less than  $100 \mu\text{J}$  over  $100 \mu\text{sec}$  before the main laser pulse. The former is generally called prepulse energy emanating from the oscillator while the latter is due to amplified spontaneous emission (ASE) from the amplifier chain. Either one of these pulses can puncture, deform, evaporate, or transform the target into a plasma of undesirable characteristics for the actual laser fusion experiments.

While ASE is easily detected and may be controlled by large aperture Pockels cells<sup>12</sup> near the output of the laser, prepulse detection and suppression is more complex. Frequently, the most detrimental prepulses occur within the last nsec before the main pulse. In this region, detection of such prepulses is extremely difficult due to the dynamic range and bandwidth requirements placed upon the detection system. Active suppression is made difficult by the fast rise time and high contrast requirements placed on the Pockels cell system.

The standard prepulse suppression implemented on most high power lasers has involved saturable dye cells in the initial portion of the laser system. The fast response times of these dyes easily fulfill the bandwidth requirements. However, saturable dyes also tend to adversely affect the overall laser beam quality by enhancing structure (modulation) already present in the spatial and temporal intensity distributions. Furthermore, dyes are more effective for short pulse operation ( $\leq 150$  psec) due to their relatively high bleaching thresholds.

At the Laboratory for Laser Energetics we have developed an alternate, completely opto-electronic prepulse suppression scheme<sup>13</sup>. It utilizes a fast optically triggered Silicon (Si) high voltage (HV) switch<sup>14</sup>, based on Auston's low voltage solid state switch<sup>15,16</sup>, to provide a very fast rise time HV pulse to a Pockels cell switchout system. The very fast rise time and low jitter of the Si switch allows opening of the Pockels cell switchout system very close to the leading edge of the desired pulse in the mode-locked train. Recent improvements of this switch have allowed practically jitter free operation of psec streak cameras<sup>17</sup> and ultrafast Pockels and Kerr cells.<sup>18,19</sup> This was made possible by the ability to switch quasi DC or DC high voltage with  $\leq 1$  psec jitter.

The Si switch providing the HV pulse consists of nearly pure (intrinsic) Si ( $30 \text{ k}\Omega\cdot\text{cm}$ ), 10 mm long, 1 mm wide, 0.5mm thick, replacing part of the central conductor

of an HN connector. Electrodes are applied on one side of the crystal with a 2 to 3mm gap in between. Without incident light the switch impedance is  $100\text{k}\Omega$ . Through a window in the connector a single  $1.054\mu\text{m}$  laser pulse activates the switch. This produces electron-hole pairs in the bulk of the Si wafer and reduces its impedance to levels much below that of the charging and transmission cables.

In practice, about  $50 \mu\text{J}$  of light energy are sufficient for full (i.e.,  $\sim 90\%$ ) HV switching. The switch stays in the ON state during the carrier recombination time of  $\sim 20 \mu\text{sec}$ . Its rise time is determined by the laser pulse duration, impedance mismatch in the switch, electrical dispersion in the cables and Pockels cells, and the optical trigger energy. Under optimum conditions, the rise time is approximately equal to the optical pulse width at half maximum, e.g.,  $\sim 30$  psec rise time for a 30 psec (FWHM) laser pulse. In order to obtain the 4 kV electrical pulse utilized in this application, 8 kV must be applied to the switch.

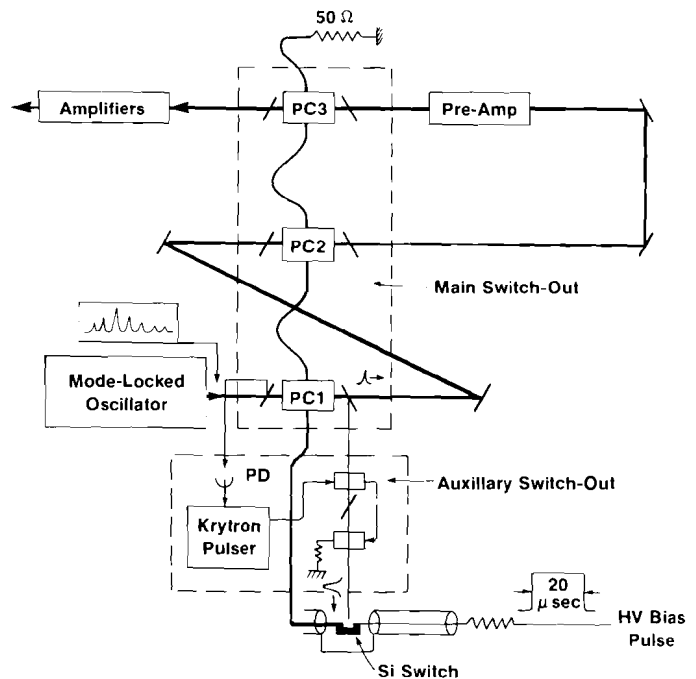


Figure 16 High precision single pulse switch-out system on ZETA. Pockels cell PC1, PC2, and PC3 are timed for optimum synchronization of the single optical pulse and the HV electrical pulse. The auxiliary switch-out uses a conventional HV pulser to select a single pulse from the mode-locked train which then drives the HV high precision Si switch.

Due to the thermal characteristics of Si and its finite initial gap impedance the HV on the charge line can only be applied for a finite time before thermal carrier excitation activates the switch. We therefore apply to the charge line a flat-top HV pulse of 50 to 100 nsec rise time and of 20  $\mu$ sec duration. The pulse duration easily accomodates the 3  $\mu$ sec jitter encountered in the emission time of most mode-locked oscillators.

The main features of the single pulse switch-out and pre-pulse suppression system are shown in Figure 16. This switch-out system is placed between the mode-locked oscillator and the amplifier chains of the University of Rochester's 3TW, ZETA laser system. The effect of this switching system on a typical laser pulse is demonstrated in Figure 17. The pulse shape of a 40 psec (FWHM) pulse was measured over 10 orders of magnitude and over 1 nsec range by means of third harmonic correlation crystal techniques<sup>20</sup>. When the overall transmission of the high speed switching system is folded in with the oscillator produced pulse shape, the calculated output pulse shape shown in Figure 17 is produced. Note that the processed pulse exhibits a power contrast (peak pulse power/pre-pulse power) of  $10^{11}$  at 400 psec before the peak of the pulse, whereas the initial pulse has a power contrast at that point in time of only  $10^6$ .

The high contrast attained by this technique has greatly improved the reproducibility of the data obtained on the ZETA and GDL laser systems.

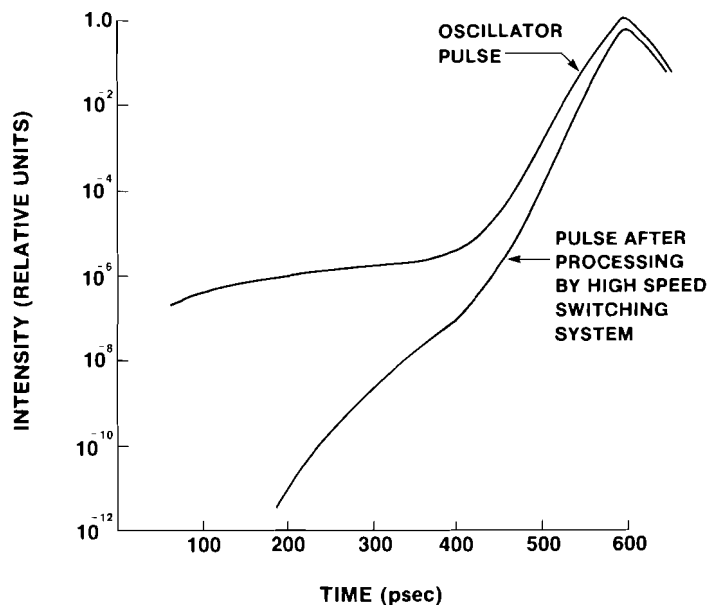


Figure 17 The measured oscillator pulse shape for the 40 psec pulse (FWHM) compared with the calculated shape after processing by high speed switching system.

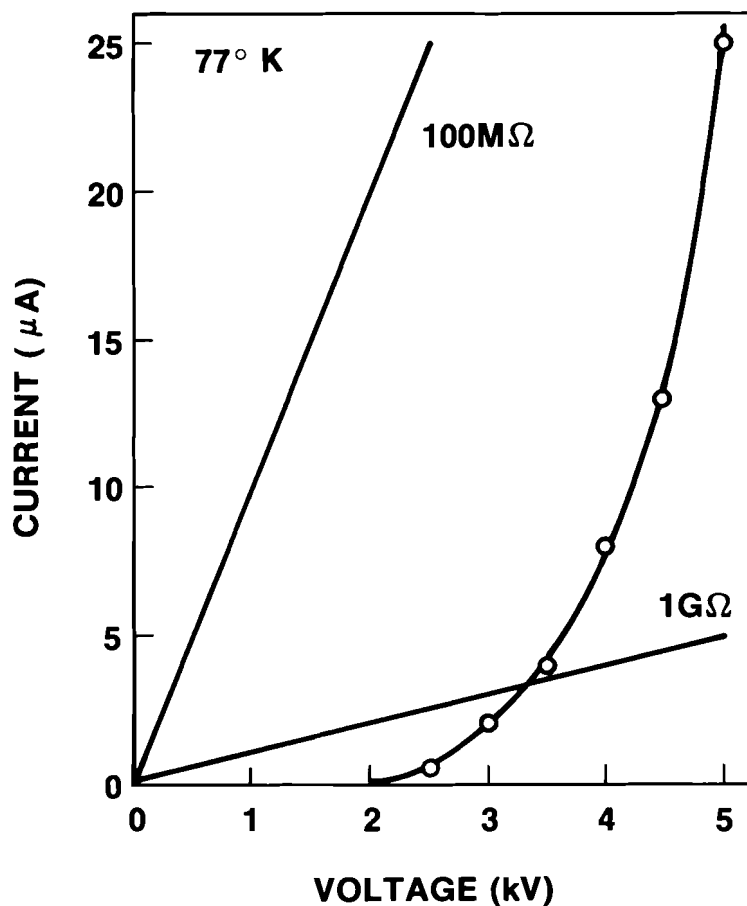
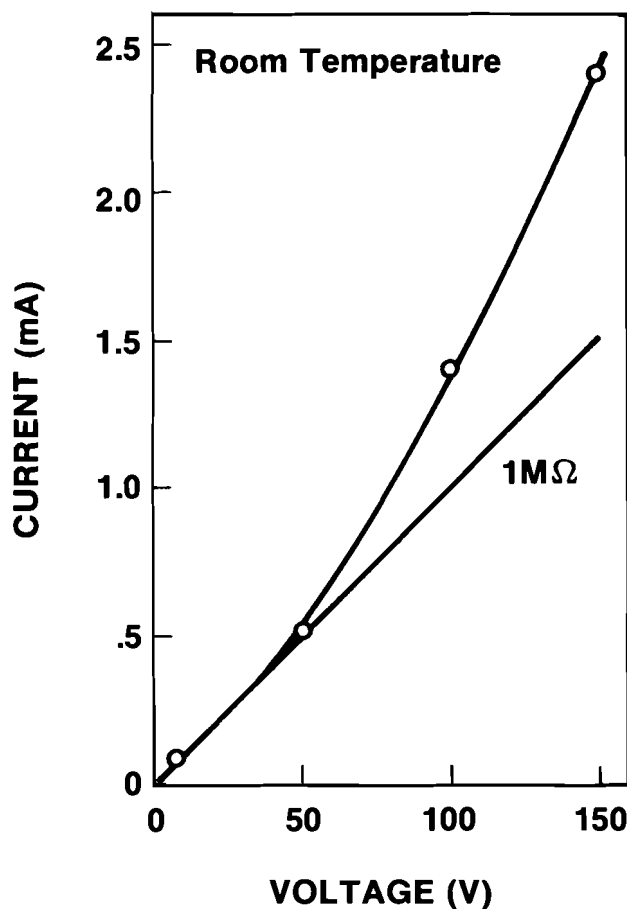


Figure 18 Current-voltage characteristics for a Au-doped Si switching element at room and liquid nitrogen temperatures demonstrate the improvement in DC holdoff as the temperature is lowered for a 2mm gap. Joule heating and the resultant thermal generation of carriers gives these curves their shape.

### 3.B Picosecond Switching of a Multi-Kilovolt DC Bias with Laser Activated Silicon at Low Temperature

For the high speed switching described above, the Si wafer was biased with a 20  $\mu$ sec HV pulse to avoid activation of the switch by thermal carrier excitation. This technology has recently been extended to include the switching of multi-kilovolt DC biases with Au-doped Si at cryogenic temperature<sup>21</sup>.

Electro-optic devices working in the picosecond domain often require picosecond switching synchronism and excellent voltage amplitude stability. Signal averaging with a streak camera<sup>22</sup> is one example where amplitude fluctuations of less than 1% are required. This constraint precludes the use of pulse bias techniques in many cases because of the shot to shot voltage variation and the timing fluctuation between the laser and the high voltage bias pulse. An additional bonus with the DC switching at cryogenic temperature is the possibility of attaining kHz repetition rates.

Nearly intrinsic Si ( $20 \text{ k}\Omega \bullet \text{cm}$ ) as is used in pulsed bias room temperature switching devices was found to be an unacceptable switching element at liquid nitrogen temperature. At low voltage a ten-fold increase in resistivity was observed followed by a premature bulk dielectric breakdown that was monitored on a nanosecond time scale for an electric field strength of  $\sim 1000 \text{ V/cm}$ . This behavior was consistently observed for 100  $\mu\text{m}$  and 2mm gaps. For the 100  $\mu\text{m}$  gap sample a Si disk with electrodes

on opposite sides was used, eliminating the possibility of surface breakdown. An interpretation of these results is that at low temperature, the freezing out of phonon motions in pure Si increases the mean free path of the carriers so that the carrier kinetic energy can exceed the impact ionization energy even for small electric field strengths, leading to a dramatic reduction of the dielectric breakdown field strength from 300 kV/cm to 1 kV/cm.

To enhance the dielectric breakdown field strength at liquid nitrogen temperature we used Si doped with deep lying Au impurities to decrease the carrier mean free paths. Au impurities were selected because donor and acceptor levels are both close to the Fermi level, .16 eV and .035 eV respectively. At room temperature the sample resistivity was  $> 3 \text{ k}\Omega \bullet \text{cm}$ . The Au concentration was estimated to be  $10^{15}/\text{cm}^3$ .

The current-voltage characteristics for a Au-doped Si switching element are displayed in Figure 18 for both room and liquid nitrogen temperatures. The gap size is 2mm. The resistivity is enhanced by several orders of magnitude upon cooling, putting the thermal runaway threshold in the kV range. We note that the low temperature dielectric breakdown field strength has been increased so that thermal effects limit voltage hold off capabilities as in room temperature switching devices.

The switching performance of a 2mm gap, Au-doped Si switching element at liquid nitrogen temperature was examined. Efficient switching was observed for applied voltages of up to 4 kV with optical turn on energies of  $\sim 50 \mu\text{J}$ . Figure 19 shows a typical pulse generated by laser induced photoconductivity switching in Au-doped Si.

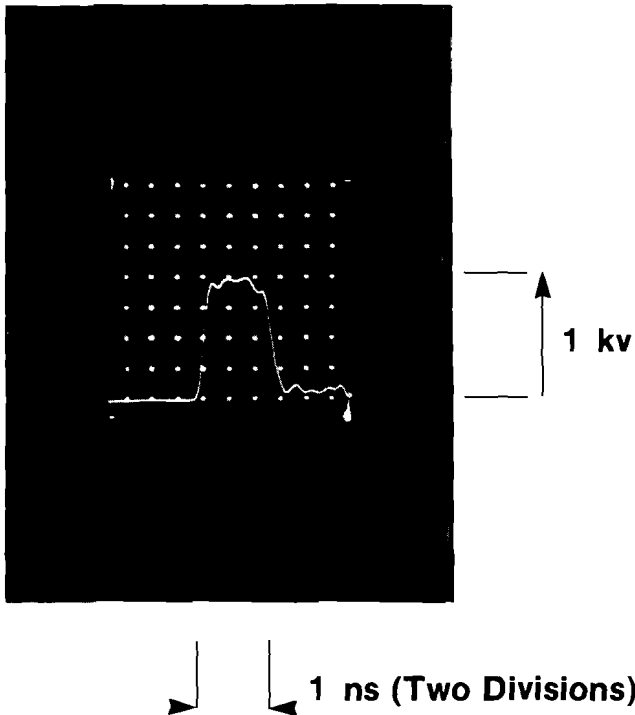


Figure 19 A typical voltage pulse generated by laser induced photoconductivity switching in Au-doped Si.

## **Section 4**

# **NATIONAL LASER USERS FACILITY NEWS**

LLE is negotiating with the Department of Energy for funding for user experiments. In order to minimize the time for obtaining funds, it has been agreed that this year user proposals should be split into two phases: Phase I would cover work preliminary to the actual experiment, that would in general be performed at the user's home institution; Phase II would cover the experiments at the National Laser Users Facility. By splitting proposals in this way it is expected that Phase I user funding will be initiated without waiting for all contract negotiations to be completed.

A meeting was held on February 14, 1980 at LLE at which this change was explained to users whose proposals have been approved by the NLUF steering committee. These users have subsequently submitted Phase I proposals. In addition, the users meeting provided an opportunity to discuss the engineering requirements of each proposal. The constraints imposed by the target chamber and the engineering discipline required at the NLUF were explained to the users. A preliminary schedule for experiments was formulated.

# PUBLICATIONS AND CONFERENCE PRESENTATIONS

## December, 1979 - February, 1980

### Publications

1. "Focusing X-Ray Spectrograph for Laser Fusion Experiments," B. Yaakobi, R.E. Turner, H.W. Schnopper, and P.O. Taylor; *Rev. of Sci. Instr.* **50**, 1609 (1979).
2. "Effect of Electrostatic Fields on Charged Reaction Products in 6-Beam Symmetrical Implosion Experiments," Y. Gazit, J. Delettrez, T.C. Bristow, A. Entenberg, J. Soures; *Phys. Rev. Lett.* **43**, 1943 (1979).
3. "A Simple Rezoning Technique for Use with the Flux-Corrected Transport Algorithm," R.S. Craxton and R.L. McCrory; *J. Comp. Physics* **33**, 432 (1979).
4. "Measurements of Brillouin-Backscatter Dependence on Density-Scale Lengths Near Critical Density," Robert E. Turner and Leonard M. Goldman; *Phys. Rev. Letters* **44**, 400 (1980).
5. "High-Power Phosphate-Glass Laser System: Design and Performance Characteristics," W. Seka, J. Soures, O. Lewis, J. Bunkenburg, D. Brown, S. Jacobs, G. Mourou, and J. Zimmerman; *App. Opt.* **19**, 409 (1980).
7. "High Density Effects on Thermonuclear Ignition for Inertially Confined Fusion," Stanley Skupsky; submitted to *Phys. Rev. Letters*.

### Conference Presentations

1980 Topical Meeting of Inertial Confinement Fusion, February 26-28, 1980. San Diego, California.

1. "Microradiography and Microdensitometry Using the Scanning Electron Microscope," H.W. Deckman and J. Dunsmuir.
2. "Microfabrication of Hemispheres from Microspheres for Structured Fusion Targets," I.S. Goldstein.
3. "A Drill and Plug Technique for Filling Laser Fusion Targets," H.W. Deckman, J. Dunsmuir, and G.M. Halpern.
4. "Self-Consistent, Non-Destructive Measurements of Tritium Content and Wall Thickness of Glass Microballoon Laser Fusion Targets," G.M. Halpern.
5. "The Coating of Fusion Targets Using Inorganic and Organic Colloidal Systems," D.G. Peiffer, H.W. Deckman, J. Dunsmuir, and T.J. Corley.
6. "Physical Vapor Deposition Coating of Gas-Levitated Fusion Targets at Low Pressures," I.S. Goldstein and J. Varon.
7. "Improvements on Parylene Coating of Fusion Targets by Molecular Structure Changes," D.G. Pfeiffer and T.J. Corley.
8. "Short-Pulse, High Power, Target Designs to Achieve Ignition Threshold Conditions," S. Skupsky, R.L. McCrory, S. Craxton, and B. Yaakobi.
9. "A Fluid First Wall/Fluid Blanket ICF Fusion-Fission Hybrid Reactor," R.T. McGrath, D.H. Berwald and J.A. Maniscalco.
10. "Computerized Analysis of Microballoon Wavefront Data," Thomas F. Powers and Gerald M. Halpern.
11. "A Dynamic Model of Optically Pumped Large Aperture Amplifiers," John H. Kelly, David C. Brown, and Kenneth Teegarden.
12. "OMEGA Booster Staging Options," D.C. Brown, J. Abate, J. Kelly, J. Hoose, and J. Waldbillig.
13. "Type II/Type II Angle Tuned Third Harmonic Generation in KDP," Stephen D. Jacobs, Joseph E. Rizzo, and Robert Boni.

### Submitted for Publication

1. "Laser Fusion Breeder Fueled Electricity Generation Systems," David H. Berwald, James A. Maniscalco; submitted to *Nuclear Technology*.
2. "An Economics Method for Symbiotic Fusion-Fission Electricity," David H. Berwald and James A. Maniscalco; submitted to *Nuclear Technology*.
3. "A Simple Silicon Switch-Driven Psec. Streak Camera," W. Knox, W. Friedman, G. Mourou; accepted by *App. Phys. Lett.*
4. "Two-Dimensional Calculations of Non-Spherical Laser Fusion Implosions," R.S. Craxton and R.L. McCrory; submitted to *Nuclear Fusion*.
5. "Laser Cross Linking of RNA Polymerase and DNA," Catherine A. Harrison, Douglas H. Turner, Jack Wilson, Mark A. DeWyngaert, and David C. Hinkle; submitted to *Journal of American Chem. Society*.
6. "Symmetric Laser Compression of Argon-Filled Shells to Densities of 4-6 g/cm<sup>3</sup>," B. Yaakobi, S. Skupsky, R.L. McCrory, C.F. Hooper Jr., H. Deckman, P. Bourke, J.M. Soures; submitted to *Phys. Rev. Letters*.

## PUBLICATIONS AND CONFERENCE PRESENTATIONS

14. "Active Mirror Amplifier Multi-Unit Performance," J. Abate, L. Lund, D. Brown, S. Reformat, and S. Jacobs.
15. "Plastic-Coated Glass Microballon Implosion Experiments," E. Thorsos, W. Seka, R. McCrory, T. Bristow, J. Delettrez, A. Entenberg, W. Friedman, S. Letzring, J. Rizzo, J. Soures, and B. Yaakobi.
16. "Direct Measurement of High Density Achieved in Symmetric Compression of Radiationally Cooled Targets," B. Yaakobi, R.L. McCrory, S. Skupsky, H. Deckman, C.F. Hooper Jr., P. Bourke, T.C. Bristow, W. Seka, J. Delettrez, and J. Soures.
17. "Symmetrical Implosion Experiments with Exploding Pusher Targets at the University of Rochester," T.C. Bristow, J. Delettrez, A. Entenberg, W. Friedman, Y. Gazit, S. Letzring, W. Seka, J. Soures, E. Thorsos, and B. Yaakobi.
18. "Liquid Crystal Isolator for Fusion Lasers," Stephen D. Jacobs, Karen A. Bauer, Richard P. Bossert, and James M. Rinefierd.
19. "New Saturable Absorbers at 1  $\mu\text{m}$ ," Stephen D. Jacobs, Joseph A. Abate, and Karen A. Bauer.

## REFERENCES

1. K. Estabrook and W.L. Kruer, *Phys. Rev. Lett.* **40**, 42 (1978).
2. J.A. Armstrong, N. Bloembergen, J. Ducuing, and P.S. Pershan, *Phys. Rev.* **127**, 1918 (1962).
3. B.H. Ripin, F.C. Young, J.A. Stamper, C.M. Armstrong, R. Decoste, E.A. McLean, and S.E. Bodner, *Phys. Rev. Lett.* **39**, 611 (1977).
4. R.E. Turner and L.M. Goldman, *Phys. Rev. Lett.* **44**, 400 (1980).
5. K. Estabrook and W.L. Kruer, *Phys. Rev. Lett.* **40**, 42 (1978); W.L. Kruer, *Phys. Fluids* **22**, 1111 (1979).
6. M.D. Rosen and J.H. Nuckolls, *Phys. Fluids* **22**, 1392 (1979).
7. E. Thorsos (editor), *LLE Review*, **Vol. I** (September-November 1979).
8. R.J. Mason and R.L. Morse, *Nucl. Fusion* **15**, 935 (1975).
9. S. Skupsky, "High-Density Effects on Thermonuclear Ignition for Inertially Confined Fusion," submitted to *Phys. Rev. Lett.*
10. J. Nuckolls, L. Wood, A. Thiessen, and G. Zimmerman, *Nature* **239**, 139 (1972).
11. J. Nuckolls, *Conference on Inertial Confinement Fusion*, February 26-28, 1980, San Diego, California, paper WA1.
12. W. Seka, J. Soures, O. Lewis, J. Bunkenburg, D. Brown, S. Jacobs, G. Mourou, and J. Zimmerman, *Appl. Optics* **19**, 409 (1980).
13. G. Mourou, J. Bunkenburg, and W. Seka, "Electro-optic Prepulse Suppression for Fusion Laser Systems," submitted to *Appl. Phys. Lett.*
14. G. Mourou and W. Knox, *Appl. Phys. Lett.* **35**, 492 (1979).
15. D.H. Auston, *Appl. Phys. Lett.* **26**, 101 (1975).
16. P. LeFur and D.H. Auston, *Appl. Phys. Lett.* **28**, 21 (1979).
17. J. Agostinelli, G. Mourou, C.W. Gabel, *Appl. Phys. Lett.* **35**, 731 (1979); G. Mourou and W. Knox, *Appl. Phys. Lett.* **36**, 623 (1980).
18. A. Antonetti, M.M. Malley, G. Mourou, and A. Orszag, *Opt. Comm.* **23**, 435 (1977).
19. M. Stavola, J. Agostinelli, and M. Sceats, *Appl. Optics* **24**, 4101 (1979).
20. G. Albrecht, A. Antonetti and G. Mourou, "The Temporal Shape of a Mode Locked Laser Pulse over Ten Orders of Magnitude," to be submitted to *Opt. Comm.*
21. M. Stavola, M.G. Sceats, and G. Mourou, "Picosecond Switching of a Multi-Kilovolt DC Bias with Laser Activated Silicon at Low Temperature," submitted to *Opt. Comm.*
22. G. Mourou and W. Knox, *Appl. Phys. Lett.* **36**, 623 (1980).